# LHCb-PAPER-2020-005 supplementary material

The angular efficiency of the 2016 data set is shown in Fig. 1. Similar distributions are seen for the other data sets used in this analysis. The long and downstream efficiencies differ due to differences in the detector acceptance between the two classes of candidates. The invariant mass and angular distributions of selected $B^0 \to J/\psi\, K^0_S$ decays are shown in Fig. 2. The mass fit is used to background subtract the data. The background-subtracted angular distribution is well described by the product of

$$\frac{\mathrm{d}^5\Gamma[B^0 \to J/\psi\, K^0_S]}{\mathrm{d}\vec{\Omega}} \propto \sin^2\theta_l \tag{1}$$

and the detector efficiency derived by simulation. Equation 1 is equivalent to setting $M_1 = \frac{1}{2}$ and $M_2$–$M_{34}$ equal to zero the angular distribution defined by Equation 2 in the LHCb-PAPER-2020-005. Figure 3 shows the $p\pi^-$ and the $\mu^+\mu^-$ mass of selected $\Lambda^0_b \to J/\psi\, \Lambda$ candidates.

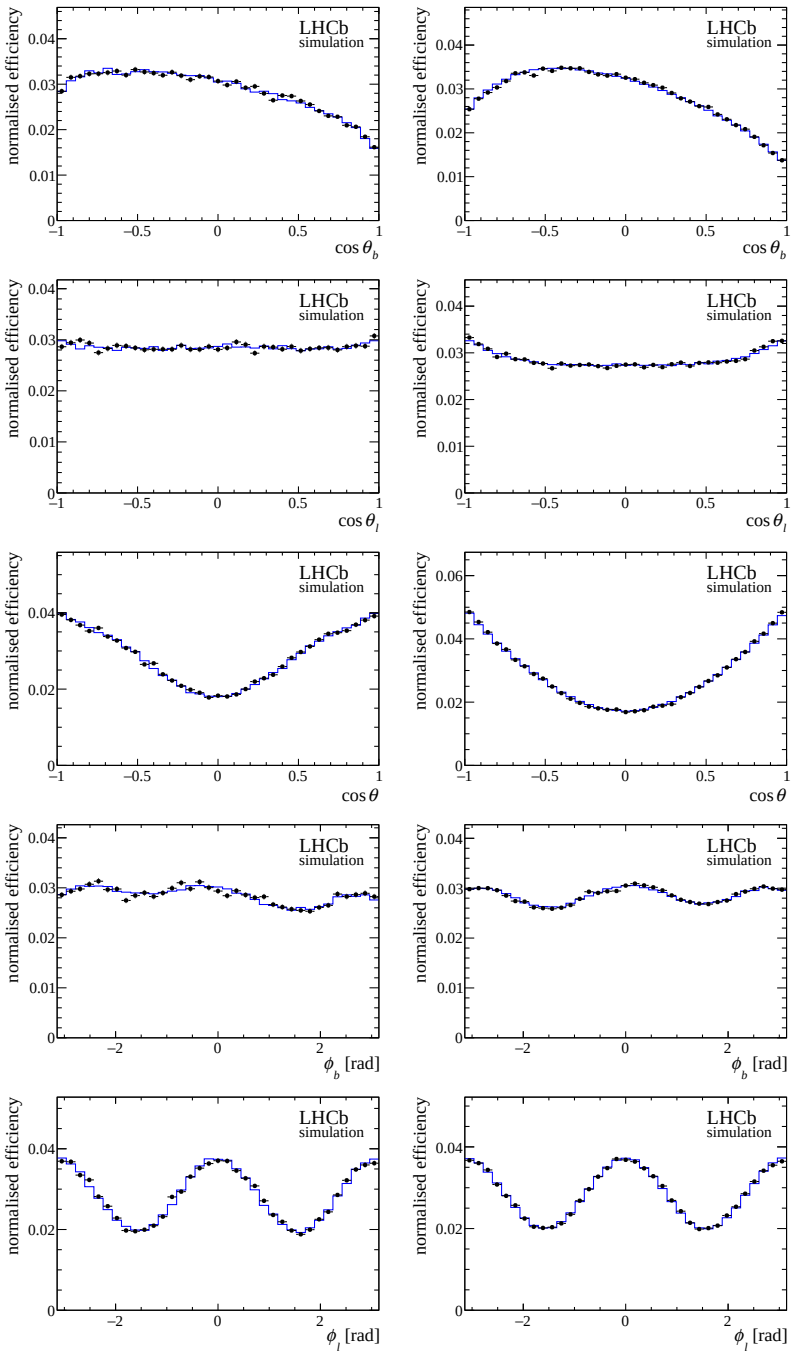


Figure 1: Angular projections of simulated phase-space decays, compared to the result of the efficiency model for (left) long and (right) downstream candidates in the 2016 data set. The data points represent the simulated candidates and the line represents the efficiency model.

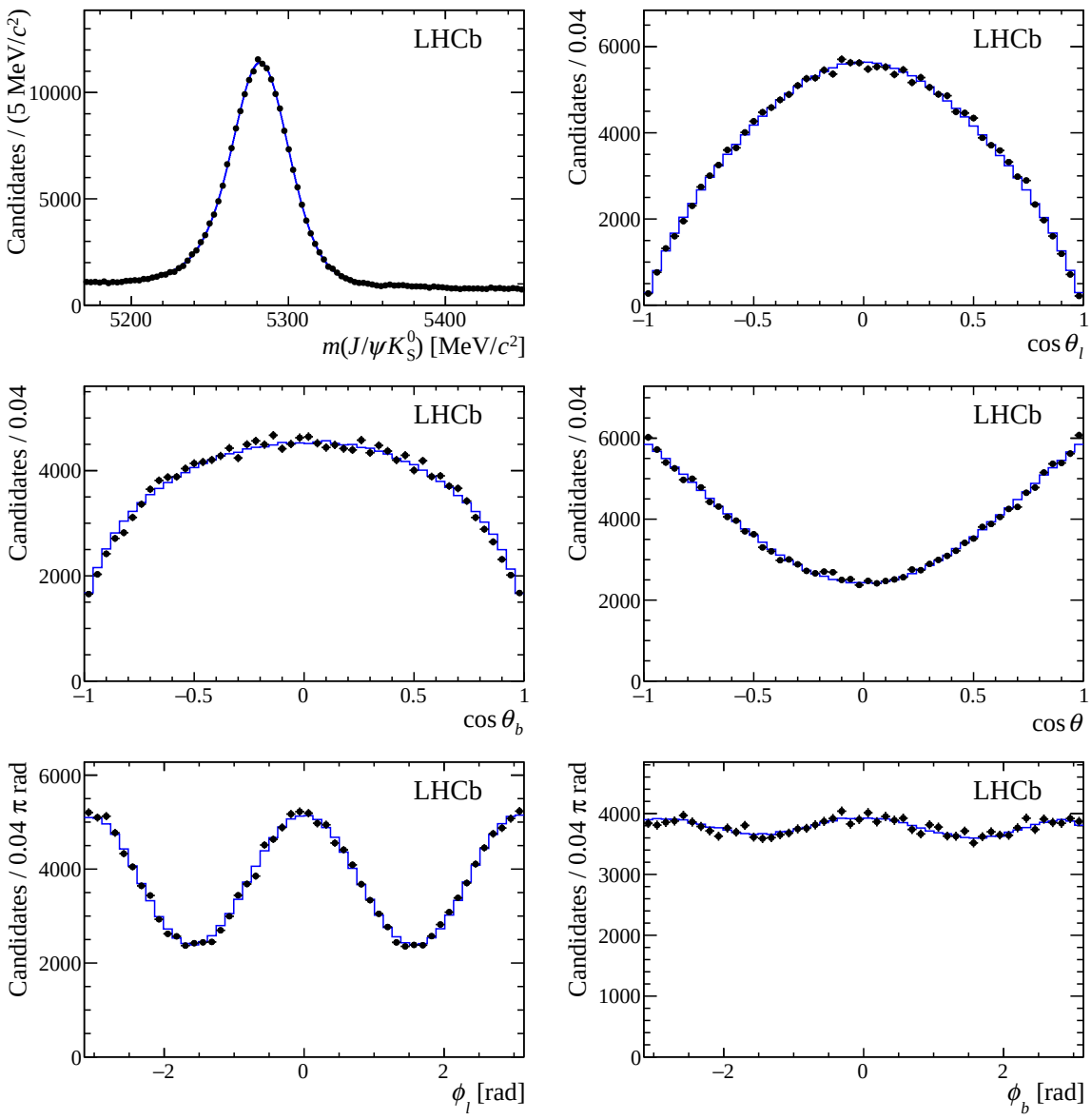


Figure 2: Invariant mass and angular distributions of selected $B^0 \to J/\psi K^0_S$ decays. The long and downstream categories and the different data taking years have been combined. The angular distribution has been background-subtracted and is compared to the result of the moment analysis, folded with the angular efficiency.

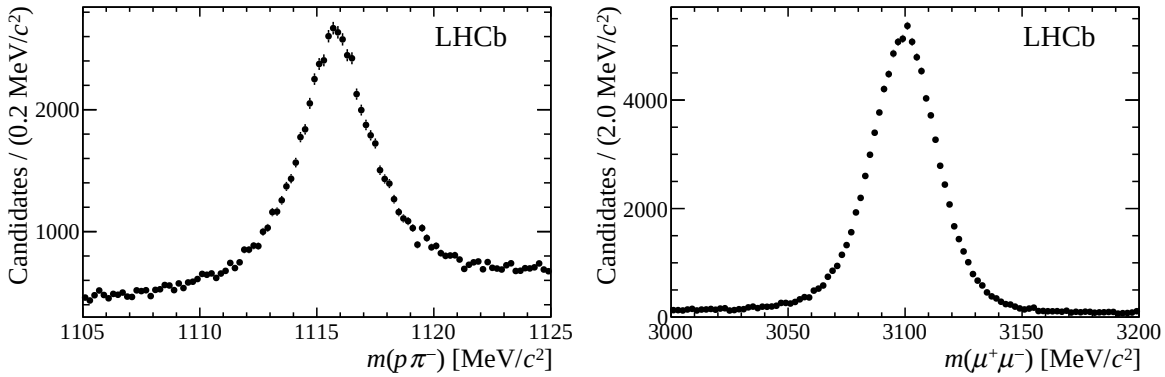


Figure 3: The (left) $p\pi^-$ and (right) $\mu^+\mu^-$ mass of selected $\Lambda_b^0 \to J/\psi\,\Lambda$ candidates before the application of the multivariate selection. Candidates in the long and downstream categories have been combined.